IJISET - International Journal of Innovative Science, Engineering & Technology, Vol. 8 Issue 11, November 2021
ISSN (Online) 2348 – 7968 | Impact Factor (2020) – 6.72
www.ijiset.com

Land Cover, Land Surface Temperature and Geomorphology Structure at Tulehu Geothermal Area, Ambon, Indonesia

Salman Hamja Siombone[1*], Jufri[2], Wiyono[3], and M. U. Syaid Maba[4]

[1]Departement of Mathematics and Natural Science Education, STKIP Gotong-Royong Masohi, Masohi 97514, Indonesia

[2]Departement of Mathematics and Natural Science Education, Darussalam University, Ambon 97582, Indonesia

[3]Department of Physics, Faculty of Mathematics and Science, Brawijaya University, Malang 65145, Indonesia

[4]Undergraduate Program of Chemistry, Faculty of Mathematics and Science, Pattimura University, Ambon 97128, Indonesia

Abstract

Research using Landsat-8 satellite imagery has been carried out to investigate land cover, land surface temperature (LST), and geomorphology structures at locations that have geothermal potential in Tulehu Village. The study area's land cover and land surface temperature were studied using multispectral image data and thermal infrared images on Landsat-8. Study geomorphological structures conducted by making 2D morphometric maps, composite band maps, and rosette diagrams. Based on the calculation results, it was found that the average value of land cover in the study area from 2015, 2016, to 2017 was 0.380, 0.396, and 0.433. While the average value of the temporal changes in LST from 2015, 2016, to 2017 was 24.474, 20.743, and 25.167. Temporal changes of LST in the study area tend to be influenced by land cover changes. Geomorphological studies using 2D morphometric maps for visual delineation show that the lineament lanes of geothermal manifestations are correlated with the shape of the slopes of the valley lineament. The composite map band-567 shows the geological features of the surface; the band-653 composite map shows land cover features, while the composite map band-742 can highlight mineral and rock aspects on the surface. The results of the lineament analysis on the rosette diagram show that several dominant fault structures control the existence of geothermal manifestations in the study area with Northwest-Southeast and Southwest-Northeast orientations.

Keywords: *Land Cover, Land Surface temperature, Geomorphology Structure, Geothermal Manifestation, Fault, and Valley Lineament.*

1. Introduction

Tulehu is a village in the Salahutu sub-district, Central Maluku district, Maluku province, Indonesia. This village has a large area and is directly adjacent to the Waai village (north), Tengah-Tengah village (southeast), Tial village (South), and Suli village (Southwest). Tulehu village is one of the villages located on the east coast of the island of Ambon [1]. Besides, Tulehu village is one of the areas on the island of Ambon that has geothermal potential. Geothermal potential in Tulehu based on the results of the Monte Carlo analysis is estimated at 30 MW [2], [3]. This geothermal potential is marked by the presence of several hot springs, which are classified into two groups based on their location, namely hot springs around Mt. Eriwakang and the hot springs around Mt. Terang Alam (Mt. Huwe). Manifestations around Mt. Eriwakang include hot springs in the Sila area, the Telaga Biru area, the Hatuasa-Karkuri area, and the Mamokeng area. At the same time, the manifestations around Mount Huwe are on Batu Kuda and Batu Lompa [2]. The hot springs of Hatuasa-Karkuri and Telaga Biru-Sila are located in the northwest part of Tulehu Village. In contrast, the Batu Kuda and Batu Lompa hot springs are located in the southeastern part of Tulehu Village. The surface temperature of the Hatuasa hot spring is 56°C, the Karkuri hot spring is 44°C, the Sila hot spring is 61°C to 100°C, the Momokeng hot spring is 40°C to 43°C, while the Batu Kuda hot spring is 52.5°C to 53°C. In addition to hot springs, the product of the geothermal manifestations formed is the alteration of rocks around the geothermal manifestations of the Hatuasa area.

Based on geological information, the hot springs in Tulehu village are thought to be controlled by the fault structure that crosses the village [1], [2]. There are three faults estimated across the village of Tulehu, and the faults are trending northeast-southwest, namely the Banda-Hatuasa fault, the Banda fault, and the Huwe fault. In addition, two faults flank the

Tulehu village boundary, which is trending northwest-southeast, namely the Tulehu fault and the Yari river fault. Several hot springs are lined up around the Banda fault and the Banda-Hatuasa fault lane, namely hot springs in the Sila-Telaga Biru area, hot springs in the Hatuasa area, hot springs in the Karkuri area, and hot spring in the Mamokeng area. Besides, several hot springs are at the northwest end of the Huwe fault, namely in the Batu Kuda and the Batu Lompa areas. In addition, on the east coast of Tulehu village, there is the Tulehu fault. This fault has orientation southeast to northwest. There is a confluence of the Tulehu fault with the Banda fault on the coast beach of Mamokeng Tulehu. A long of Tulehu fault, there are several hot springs, started from Batu Lompa to the coast of the Mamokeng area. In addition, there are several hot springs in the west of Tulehu village, at the intersection of the Banda fault and the Yari River fault, namely the Hatuing hots sping.

The faults that cross the village of Tulehu and its surroundings affect the condition of the area's landscape. The existing landscape appears in topographic undulations, ranging from coast and valleys to lowland mountains [1]. In the study area, there are two points with the highest topography, namely Mount Huwe with an altitude of ± 170 m a.s.l and mount Eriwakang with an altitude ± 330 m a.s.l (meters above sea level). In addition, there are also valleys which are fault lines or fractures around the two mountains, such as the Banda Fault, Banda Hatuasa Fault, and Huwe Fault. Geothermal manifestations in hot springs appear in the valleys along the Banda fault, the Banda-Hatuasa fault, the northwest end of Huwe fault, and the Tulehu fault. Complex landscape conditions are obstacles to direct observations (groud checks) of the existing geomorphology and geothermal prospects. One of the methods that can be used to investigate an expansive landscape that cannot be reached terrestrially is the remote sensing method [4]. Remote sensing methods can help identify features of geological structures on the earth's surface, such as lineament features, faults, valleys, hills, and other landforms [4], [5]. Remote sensing data such as Landsat-8 can map and monitor land use/land cover, land surface temperature, land surface biophysical, and geophysical properties [6]. In contrast, remote sensing data such as DEM SRTM can detect surface geological structures [7], [8]. Based on several advantages of the remote sensing method, this method is used to observe the transformation of land cover, temporal change of land surface temperature, and geomorphology structure condition in the geothermal prospect area in Tulehu village.

Fig. 1: (a) Hatuasa Hot Spring, (b) Sila Hot Spring, (c) Batu Kuda Hot Spring, and (d) Mamokeng Hot Spring

2. Study Area

This study was carried out in Tulehu Village and covered the surrounding areas. The study area was conducted in an area of 9.60 km × 9.20 km or 88.32 km^2. The study area was geographically in 52 Southern Hemisphere zones, with eastern and northern positions of 420663.00 mE to 430182.00 mE and 9597916.00 mS to 9604191.00 mS. This research focused on recap land cover transformation, temporal change of land surface temperature, and geomorphology structure condition in areas with geothermal prospects in Tulehu village. The areas with geothermal prospects are the Hatuasa-Karkuri area, the Sila area, the Telaga Biru area, the Mamokeng area, the Batu Kuda area, the Batu Lompa area, and the Hatuing area around the Yari river. The study area is shown in Figure 2.

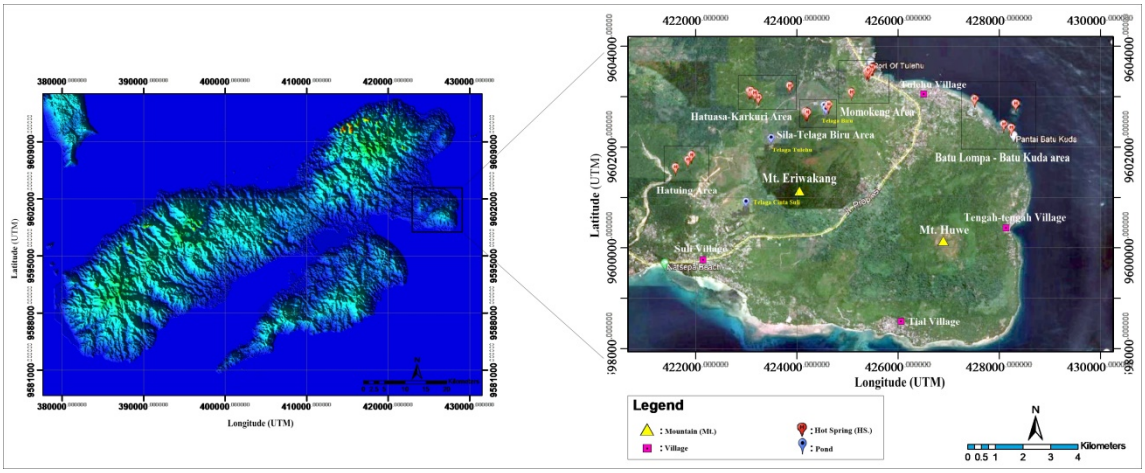

Fig. 2 Study Area of Tulehu Geothermal Prospect

3. Materials and Methodology

3.1 Data

Remote sensing data employed in this study are Landsat-8 data for path: 109 and row: 62 and DEM SRTM (Digital Elevation Model, the Shuttle Radar Topography Mission) 1 Arc-Second data. The data were secondary data downloaded on the USGS website. Furthermore, Landsat-8 data used were data recorded on September 21st, 2015, August 22th, 2016, and October 28th, 2017, with the cloud cover percentages of 0.86%, 0.50%, and 4.56%, respectively. The percentage of good cloud cover in remote sensing data processing should be <10% [9]. Landsat-8 data employed to determine land cover and estimate land surface temperature was thermal infrared images in the thermal infrared (TIR) Landsat-8 sensor and multispectral band images in operational land imager (OLI) Landsat-8 sensor. The multispectral images for processing land surface temperature consisted of band 5 (Near Infrared/NIR) and band 4 (Red). Thermal infrared images used are band 10 (TIR-1) and band 11 (TIR-2). Meanwhile, DEM SRTM data was employed to create morphometric maps surface and 2D topographic maps to study the lineaments, faults, and landforms of Tulehu village and surroundings. The lineaments and fault structures on the 2D topographic map are visually delineated with the help of the Tulehu Geological map from JICA (Japan International Cooperation Agency) research results [3]. As support, geological structure analysis requires some data from Landsat-8 images, namely multispectral images from band 6 (Short Wavelength Infrared-1/SWIR-1), band 7 (SWIR-2), band 5 (NIR), band 4 (Red), and band 3 (Green). These multispectral images are employed to make Band composites and are commonly referred to as Red Green Blue composites (RGB). The RGB composites in which are band-567 composites, band-653 composites, and band-742 composites. Respectively, these composites have advantages in geological analysis, agriculture analysis, and rock or surface minerals analysis [7], [10], [11].

3.2 Method

a. Land Cover

Land cover describes the condition of vegetation density in the study area. Land cover in an area can be calculated using the Normalized Differential Vegetation Index (NDVI) equation. The data used in the NDVI calculation is Landsat 8 multispectral image data consisting of band 4 and band 5. Before the calculation was conducted, those band images data needed to be radiometrically corrected. This correction is carried out to improve the image's visual quality by improving the pixel value and other atmospheric disturbance factors caused by the initial error of scanning by the satellite. This correction is done by changing the Digital Number (DN) value into the Top of Atmosphere (ToA) reflectance. ToA reflectance correction equation as follows [12], [13]:

$$\rho_\lambda = \frac{M_\rho \cdot Q_{\text{cal}} + A_\rho}{\sin \theta_{SE}} \qquad (1)$$

where, ρ_λ spectral reflectance (ToA reflectance) with solar angle correction, M_ρ is a scale factor multiplying band reflectance, Q_{cal} is the DN value of each pixel, A_ρ is a scale factor adding band reflectance, and θ_{SE} is the local solar elevation.

The NDVI value always ranges from -1 to +1. A value of -1 correlates with water objects or objects containing water, a value of 0 correlates with soil objects, and a value of +1 correlates with vegetation objects [9].

b. Land Surface Temperature

The land surface temperature (LST) value of an area is strongly influenced by its emissivity value. The emissivity value is an important component in the calculation of LST In addition, the calculation of the emissivity value also requires the value of the vegetation proportion (vegetation fraction). The components in the calculation of the vegetation fraction are obtained based on land cover classification concerning the range of NDVI values. The vegetation fraction value is obtained by applying the following equation [14], [15]:

$$Pv = \left(\frac{NDVI - NDVI_{min}}{NDVI_{max} - NDVI_{min}}\right)^2 \quad (2)$$

where NDVI is the NDVI value for each pixel, $NDVI_{max}$ is a representation of the NDVI of vegetation, and $NDVI_{min}$ is a representation of the NDVI of soil to water bodies. In this study, $NDVI_{max}$ is equal to or greater than 0.50, and $NDVI_{min}$ is equal to or less than 0.20.

The classification of emissivity values in this study is based on the results of research from Mia et al. (2017), namely [15]:

1) Bare land or land correlated with soil objects has a vegetation fraction value (Pv) is 0 and has an emissivity value ($\varepsilon_{soil\ land}$) of 0.98.
2) Fully vegetated land has a vegetation fraction value (Pv) of 1, and an emissivity value ($\varepsilon_{vegetated\ land}$) is 0.99.
3) Mixed land is a combination of vegetated land and bare land, and its emissivity value is determined following findings from Sabrino:

$$\varepsilon_{mixed\ land} = mP_v + n \quad (3)$$

with,

$$m = \varepsilon_{vegetated\ land} - \varepsilon_{soil\ land} - (1 - \varepsilon_{soil\ land})\, F \cdot \varepsilon_{vegetated\ land}$$
$$n = \varepsilon_{soil\ land} + (1 - \varepsilon_{soil\ land})\, F \cdot \varepsilon_{vegetated\ land}$$

where F is a shape factor that has a value of 0.55.

In addition to requiring soil emissivity values, the calculation of LST values also requires Landsat-8 thermal band image data, namely band 10 (TIR-1) and band 11 (TIR-2). The thermal band image data is processed through the calculation of Top of Atmospheric (ToA) Radiance by changing the Digital Number (D.N.) value to the radiance value, using the following equation [12]:

$$L_\lambda = M_L \cdot Q_{cal} + A_L \quad (4)$$

Where L_λ is the spectral radiance (ToA radiance) of the thermal band (W m^2 $srad^{-1}$ m^{-1}), M_L is the scale factor of the radiance multiplier of the thermal band, Q_{cal} is the DN value of each thermal pixel, A_L is the scale factor for adding up the radiance in the thermal band.

The next step is to determine the value of the brightness temperature. This step is done by changing the spectral radiance value in equation (5) into the brightness temperature value. The brightness temperature value is obtained using the following equation:

$$T_{Sensor} = \frac{K_2}{ln\left(1 + \frac{K_1}{L_\lambda}\right)} - 273.15 \quad (5)$$

Where T_{Sensor} is the brightness temperature on the sensor (°C), L_λ is the thermal spectral radiance band, K_1 is the thermal conversion constant 1 for the thermal band, K_2 is the thermal conversion constant 2 for the thermal band.

Then the LST value in the study area is calculated by the equation recommended by Jimenez-Munoz and Sabrino in Qin et al.[13], as follows:

$$T_s = \frac{T_{sensor}}{1 + (\lambda_{band10,11} \cdot \frac{T_{sensor}}{h \frac{c}{j}}) \ln \varepsilon} \quad (6)$$

Where T_s is the LST (°C) of the study area, λ is the wavelength of emission radiance, $\lambda_{Band\ 10,11}$= 11.5 m, h is Planck's constant, 6.626 × 10^{-34} Js, c is the speed of light is 2.998 × 10^8 $m.s^{-1}$, j is the Boltzmann constant, 1.38 × 10^{-23} J°C^{-1} and is the emissivity of the soil from the study area.

c. Geomorphology Structure

Geomorphology is the study of regular and random natural forms on the earth's surface and all the processes that produce these forms [16]. The study of geomorphological structures in the Tulehu geothermal area will be studied through

three main parts, namely: (1) Surface morphometric maps and visual delineation, (2) Composite of multispectral bands, and (3) Lineament manual and Rosette diagrams.

1) Map of Surface Morphometric and Visual delineation

Morphometry is a quantitative assessment of landforms as a supporting aspect of morpho-grapy and morphogenetics so that the classification becomes more assertive with exact numbers [17], [18]. In this study, surface morphometry focused on classifying slope and morphological units based on van Zuidam in 1985. The data used in this morphometric study is DEM SRTM 1 Arc-Second. The data is cropped according to the focus of the study area and then processed in the Global Mapper app at the "Dynamic hill-shading" tool according to the slope class and color classification suggested by Vain Zuidam in 1985. The classification of the slope classes is shown in Table 1.

Table 1. Classification of slope classes based on van Zuidam in 1985

Slope Class	Process identification and field conditions	Suggested color
0 deg – 2 deg	Flat or with insufficient denudational processes and less intensive surface erosion under dry conditions.	Medium-dark green
2 deg – 4 deg	Slightly sloped (*gently slope*), with a low-velocity mass movement of various periglacial processes: solifluction and fluvial.	Bright green
4 deg – 8 deg	Sloping has almost the same conditions as the gentle slope but is more prone to surface erosion, with intensive surface erosion.	Bright yellow
8 deg – 16 deg	Slightly steep (moderately steep), all types of mass movement occur, especially periglacial-solifluction, crawling, erosion, and sometimes erosion	Orange
16 deg – 35 deg	Steep, denudational processes of all types occur intensively (erosion, creep, and soil movement)	Bright red
35 deg – 55 deg	Very steep, denudational processes occur intensively.	Medium Dark red
> 55 deg	Extreme steep, rock intrusion process	Medium-dark

This study uses visual delineation to analyze geomorphological structures related to fault lanes and lineaments around the geothermal manifestation points in the study area. Visual delineation was carried out on the results of the DEM SRTM modeling, a morphometry 2D map. The delineation results on the 2D morphometric map are correlated with the Tulehu geological map for accuracy in the discussion.

2) Composite of Multispectral Bands in Landsat-8

Band composite imagery is carried out with the aim of combining the colors contained in the three bands to highlight the expected target [8]. The composite of these three bands is often referred to as the RGB (Red-Green-Blue) composite [10]. In this study, composites were carried out on several bands of Landsat-8 multispectral images. RGB band composites were performed on Arcgis 10.3. The composite maps in intending are composite maps of band-567 (geological structure target), composite map band-653 (vegetation analysis target), and composite maps of band-574 (rock mineral target) [4], [7], [11]. Before the composite band, a radiometric correction was carried out to minimize various errors in recording the reflected value of sunlight [7].

3) Lineament Manual and Rosette Diagram

Manual lineament in this study was carried out using DEM SRTM data in the Global Mapper application, using the digitizer feature in the "create line features" option. In this study, analysis was carried out on the lineaments of the valley with an azimuth of 45°and 135°. The lineament digitization data obtained is then exported to CVS format to retrieve the Stike data. In addition to the Strike data from the existing lineament, a Dip value is also needed. In this analysis, a Dip value of 90° is used for the entire data. Using Dip with a value of 90° is because it must be perpendicular from the perspective we see the map. The Stike and Dip data are then analyzed using the Dips 7.0 app to create a Rosette Diagram. The Rosette Diagram is used to know the direction or orientation of the lineaments distribution [19].

4. Result and Discussion

The results and discussion focused on data processing results regarding changes in land cover conditions, temporal changes in LST, and geomorphology structure, including visual delineation on the morphometric map, composite of the multispectral band, lineament manual, and Rosette diagram in the study area.

4.1 Land Cover

Land cover classification in the study area is divided into four types, namely (1) Body of Water (NDVI value of < 0.000), (2) Bare Land, coastal sand deposits, and Cloud Cover (NDVI Value of 0.000 to 0.200), (3) Mixed land (0.200 < NDVI < 0.500), and vegetated land (NDVI > 0.500). Based on Figure 3, the land cover in the study area is filled by the four classification types distributed according to topographic conditions and residential areas. Based on Table 2, it can be seen that in the study area, the average NDVI value from 2015, 2016, to 2017 was 0.380, 0.396, and 0.433. Sequentially the average NDVI value indicates that the study area is dominated by mixed land.

Table 2. NDVI values around Tulehu geothermal area, Ambon

No	Recorded Data	Minimum	Maximum	Average Value of the Study Area
1	September 02th, 2015	-0.317	0.602	0.380
2	August 22th, 2016	-0.260	0.594	0.396
3	October 28th, 2017	-0.319	0.601	0.433

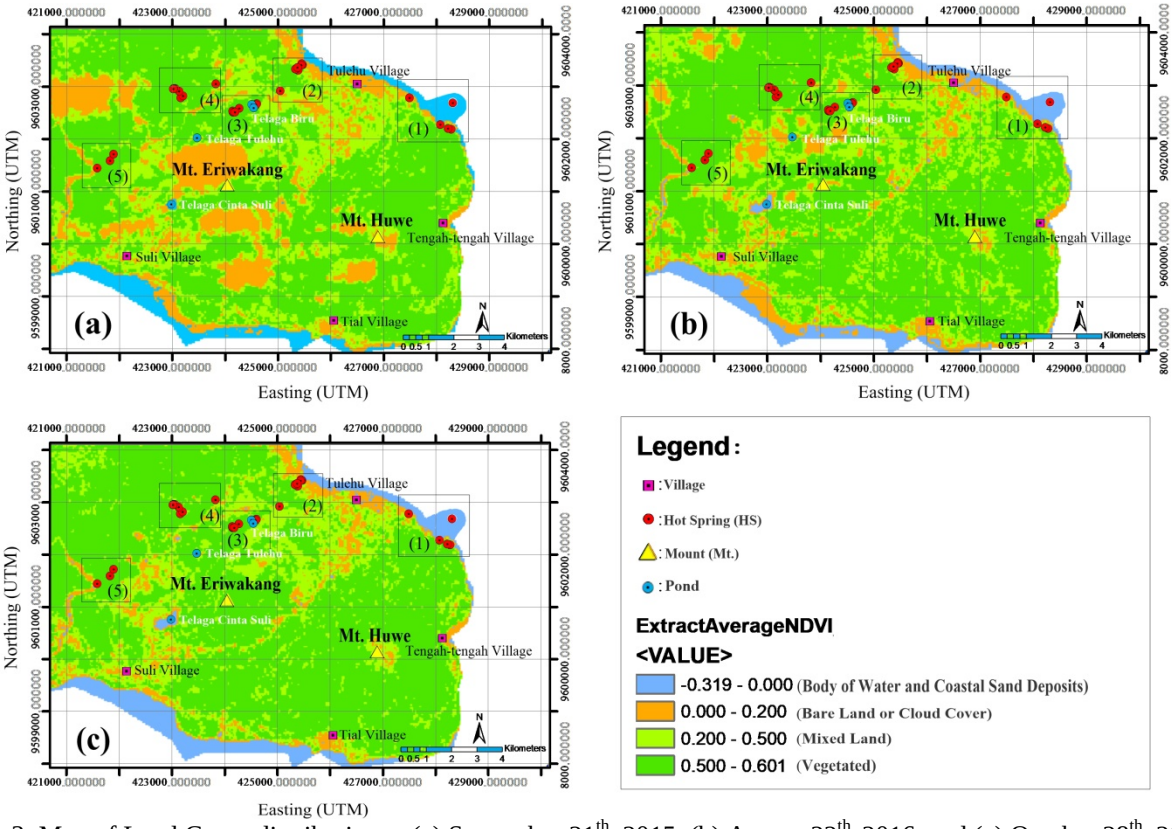

Fig. 3: Map of Land Cover distribution at (a) September 21th, 2015, (b) August 22th, 2016, and (c) October 28th, 2017

4.2 Land Surface Temperature

Land Surface Temperature (LST) is a condition that is controlled by the balance of surface energy, atmosphere, thermal properties of the surface, and soil surface media. The key to LST is emissivity, while variations in emissivity values

on the earth's surface are determined by variations in vegetation cover, composition, humidity, and surface hardness [20], [21].

As with land cover, the discussion of land surface temperature will focus on potential geothermal areas in the research area. In addition, the LST discussion will also focus on points that have high anomaly values. The temporary changes of LST in the study area are shown in Figure 4, while the average LST value in the study area is summarized in Table 3. The average LST value from 2015, 2016, to 2017 was 24.474, 20.743, and 25.167. Generally, temporal changes of the average LST value in the study area are affected by land cover.

Table 3. LST values around Tulehu geothermal area, Ambon

No	Recorded Data	Minimum	Maximum	Average Value of the Study Area (°C)
1	September 02th, 2015	17.192	31.574	24.426
2	August 22th, 2016	17.187	25.928	20.743
3	October 28th, 2017	22.119	32.362	25.167

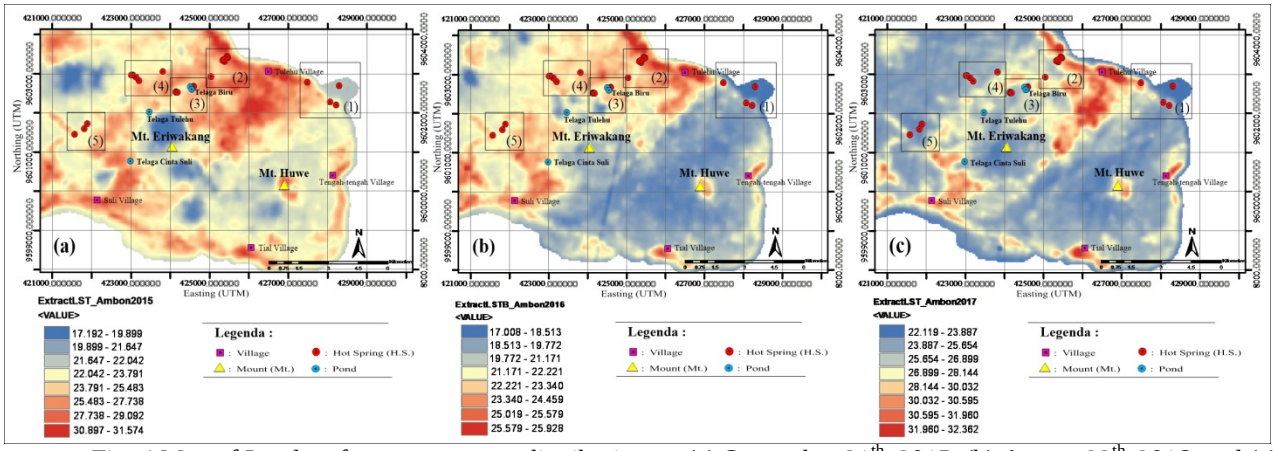

Fig. 4 Map of Land surface temperature distribution at: (a) September 21th, 2015, (b) August 22th, 2016, and (c) October 28th, 2017.

The study of LST temporal changes in the study area focuses on five locations which have geothermal potential. The areas studied were: (1) the Batu Kuda-Batu Lompa area, (2) the Mamokeng area, (3) the Sila-Telaga Biru area, (4) the Hatusa-Karkuri area, and (5) the Hatuing area (around Yari river). Based on Figure 4, it can be seen that the Batu Kuda-Batu Lompa area has a distribution trend of LST anomalies that are almost the same, except for changes in contrast in temperature from year to year. This same anomaly trend is characterized by the rhythm of increasing or decreasing the same temperature only at the same points each year. The Mamokeng area has the same distribution trend of LST anomalies, only that there is a decrease in temperature contrast from 2015 to 2017 in a row. The Sila-Telaga Biru area has a slightly different LST anomaly trend, but it is similar for 2015 and 2016 (see Figures 4. a and 4. b). The LST anomaly trend in the Sila-Telaga Biru area experienced a decrease in contrast from 2015 to 2017. The Hatuasa-Karkuri area has almost the same trend of anomalies contrast, where from year to year, points with high anomalies remain visible. In addition, the geothermal manifestation points in the Hatuasa-Karkuri area appear to have a higher LST anomaly value than the surrounding area. This is because the manifestation points in the Hatuasa area tend to be on open land (bare land). The Hatuing area had the same anomaly trend, although there was a decrease in the contrast of the LST anomaly from 2015 to 2017. In general, areas with geothermal potential generally have a low LST anomalous contrast, and this is because these areas are mostly located on vegetated land. High vegetated land cover can also reduce the effectiveness of satellites in capturing dan recording points that have geothermal potential.

Based on Figure 4, if explored further, residential centers (built-up land) areas generally have a higher contrast of LST anomalies than areas with high vegetation density. While at the top of a mountain such as Mount Huwe has the same anomalous trend from year to year with a high contrast anomaly compared to the surrounding area. The high anomaly of LST value in this mount is influenced by a condition in the top of the mountain, dominated by open land and a little mixed land. While at the top of Mount Eriwakang, there is no high LST anomaly. This is because the area around the mountain and the top of the mount are covered by densely vegetated land. Land cover changes generally affected the increase of LST

anomalies in the study area [7]. The increase of LST anomaly is also caused by human activities in land use [22], for example, the clearing of agricultural area, residential area to the administrative interests of the local community.

4.3 Geomorphology Structure

The discussion related to the geomorphological structure in this study will be described through three main components, namely: (a) Map of Surface Morphometric and visual delineation, (b) Composite of multispectral bands in Landsat-8, and (c) Lineament manual and rosette diagram.

a. Map of Surface Morphometric and Visual delineation

Surface morphometric maps are used to describe the condition of the slope class in the form of a slope and slope shape. The slope classes are classified based on the findings of Van Zuidam in 1985 (see Table 1). This study related to surface morphometry focuses on locations with geothermal manifestations (Figure 5a) and examines fault paths based on traces of hot springs and slopes (Figure 5b). The locations that became the main focus of the study consisted of five locations, namely: (1) Batu Kuda area, (2) Mamokeng area, (3) Sila-Telaga Biru area, (4) Hatusa-Karkuri area, and (5) Hatuing area.

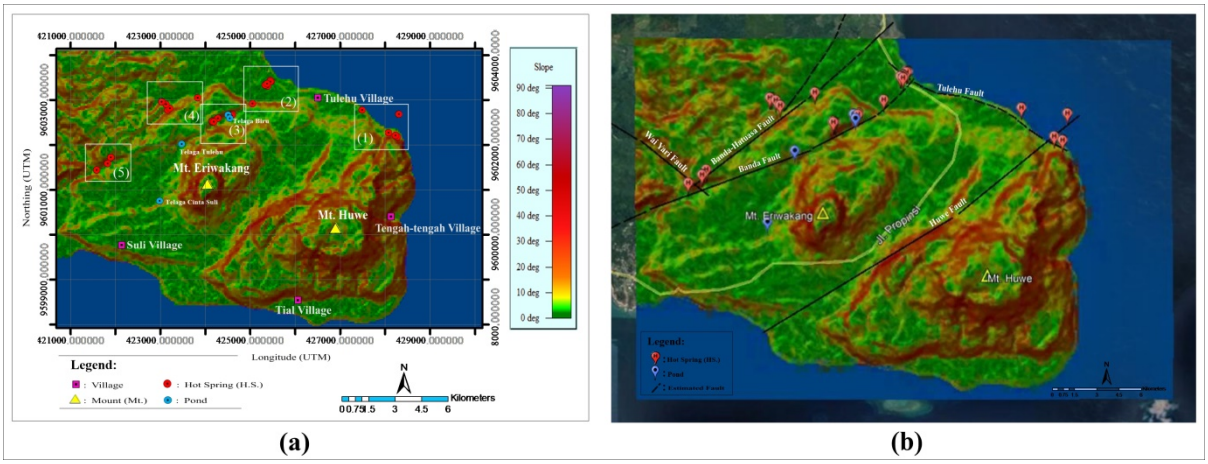

Fig. 5: (a) Mofrometric map of Tulehu geothermal area, and (b) visual delineation on the morphometric map.

The Batukuda area is on the surface with a slope of 5 deg (Bright yellow) to 50 deg (Medium Dark red). This condition illustrates that the Batu Kuda area is on the surface from a gentle slope to a very steep slope. The Mamokeng area is an area that has a slope of 0 deg (Medium-dark green) to a slope of 45 deg (Medium Dark red). A flat surface dominates the Mamokeng area, while on the border of the upper Mamokeng area with Telaga Biru, there is a hill with a very steep slope (Figure 5.a.). The Sila-Telaga Biru area is an area that has a slope from 0 deg (Medium-dark green) to a slope of 60 deg (Medium-dark). A slightly steep slope dominates the Sila-Telaga Biru area to the extreme steep. This area with a slope of extremely steep to slightly steep forms a lane southwest to northeast direction. Around the slope, a lane appears a row of several hot springs and pond valleys (such as Mataputih and Telaga Biru pond). The Hatuasa-Karkuri is an area that has a surface with a slope ranging from 0 deg (Bright green) to 30 deg (Bright red). Locations with a flat surface area in the north, while locations with a steep slope area in the southeast and south of the Hatuasa-Karkuri area. In this area, a lineament lane appears with southwest to northeast orientation. There is a line of hot springs along the lane starting from the Hatuasa area to the Karkuri area. The Hatuing area is an area that has a slope ranging from 4 deg (Bright green) to 45 deg (Medium Dark red). In general, the Hatuing area is a valley area with a slightly sloping surface to very steep. Several hot springs lined up to appear at the confluence between the lineaments of the Hatuing fault (Yari river valley) and the lineaments of the Banda fault (Figure 5. b).

Lineament is a simple or complex linear feature on the earth's surface that is mapped, has a straight or slightly curved appearance, can be distinguished from the surrounding features, and is thought to be a subsurface phenomenon. Examples of lineaments include river lineaments, geomorphological or topographic lineaments (lows or ridges), hot springs lineaments, and lineaments in geophysics (magnetic and gravity) [16]. The properties of a fault can be studied through a combination of hot spring lineaments and geomorphological lineaments, which are positively correlated. In this study, the presence of fault lines was assessed through hot spring lineaments and valley lineaments on the surface morphometric map

(Figure 5. b). Mophrometric maps can clearly show the shape of the slope around hot springs in the study area. While, in this study, visual delineation will be carried out on the structure's lineament lane, which is estimated to be a fault lane. The process of assessing the structure focuses on valley lanes with geothermal prospects in the form of hot springs. This visual delineation study for the lineament of the fault will be strengthened by an overlay of the Tulehu geological map (Figure 6) [3]. The lineaments studied were: (1) lineament of the Huwe fault, (2) lineament of the Tulehu fault, (3) lineament of the Banda fault, (4) lineament of the Banda-Hatuasa fault and (5) lineament of the Yari river fault.

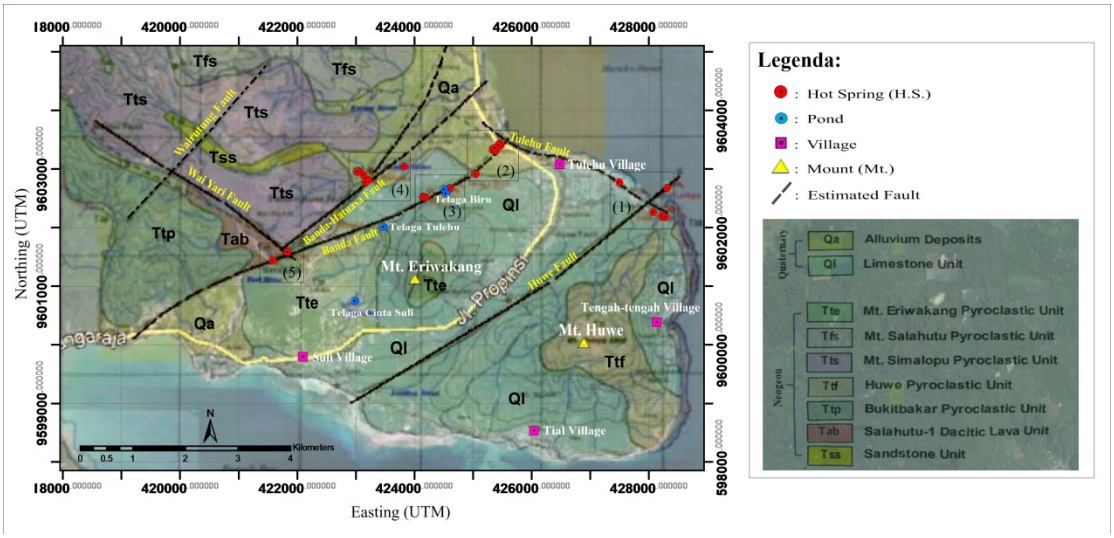

Fig. 6 Overlay of Tulehu geological map on the study area, Modified from JICA, 2011 [3]

Based on Figures 5. b and 6, the Huwe fault is located around the Huwe mountain valley in a northeast-southwest direction. At the northeastern end of the Huwe fault, several hot springs range from the Batu Lompa to the Batu Kuda area. The Huwe mountain valley along the lineament of the Huwe fault appears to have an extreme slope with a very significant topography change from flat to Extreme steep. In addition, on the Tulehu fault, the lineament is estimated to start from the Batu Kuda coast to the Mamokeng coast in a southeast-northwest direction. The lineament of the fault is on the border between a flat surface and a gentle slope on the east coast of Tulehu village. The lineament of the Tulehu fault intersects with the lineament of the Banda fault in the Momokeng beach area. The Banda fault line, on the morphometric map, a lineament lane can be drawn starting from the Yari River valley in the southwest, then towards the Tulehu pond fracture, then connected to the Sila-Telaga Biru valley, then towards the hot spring Kaget in the upper Mamokeng area, continuing towards Mamokeng swamp and ends on the coast of Mamokeng in the northeast. The continuity of the Sila-Telaga Biru hot spring lane to the Kaget hot spring, then to the Mamokeng swamp to the Mamokeng coast, and a hot spring lineament lane is clearly identified. On the morphometric map of the study area, the lineament of the Banda-Hatuasa fault can be identified through the lineament of the valley and hot springs. The fault lane starts from the Yari river valley, which continues in the Wamina river valley in the Hatuasa area. It is divided into two lanes, namely the Rutung river line on the coast of Waai village and the valley in the Karkuri area, which ends on the Hurnala II coast of Tulehu village. While on the Hatuing area, there is a lineament along the Yari River valley lane. The lineament is estimated to be a fault. The strong suspicion regarding the location of the Yari river fault is reinforced by the presence of several hot spring points in the Hatuing area.

Figure 6 is the result of overlaying the geological map of the Tulehu area in the google earth app. This overlay map is used to support and strengthen the explanation regarding the presence of fault lineaments in visual delineation (Figure 5. b). In addition, this overlay map is used to support explanations related to the geological conditions of the Tulehu area, especially in rock minerals for composite band-742 (Figure 7. c).

b. Composite of Multispectral Bands in Landsat-8

Composite bands in this study are used to examine the geomorphological features of the study area, both in terms of surface geological structures, residential areas, vegetation, and rock minerals. Geomorphological features in the study area will be examined in three composite band maps: composite band-567, composite band-653, and composite band-742. The three composite band maps have their respective advantages. Composite band-567 has advantages in displaying geological structures, and composite band-653 shows vegetation analysis (agriculture), while composite 742 has advantages in displaying minerals rocks on the surface. Several essential elements must be understood in interpreting a composite band

map, such as the color indicators to identify specific features or objects. Several color indicators in composite map band-567 were black is a body of water, brown-reddish is vegetated land, light blue is a built-up area, light green is mixed land to bare land, and the bright white is open ground. Several color indicators in composite map band-653 were black is a body of water; dark green is forest; light green is a bush or mixed land; dark green with a regular pattern is a garden; green yellowish with regular patterns are plantation fields; light brownish green is grass or bare land, and red is a residential area. Meanwhile, several color indicators in composite map band-742 were blue-dark or black is a body of water; deep dark green is forest vegetation; dark blue or pink is a residential area; the red to orange represents the different origins of various rock types, and dark brown is mixed land.

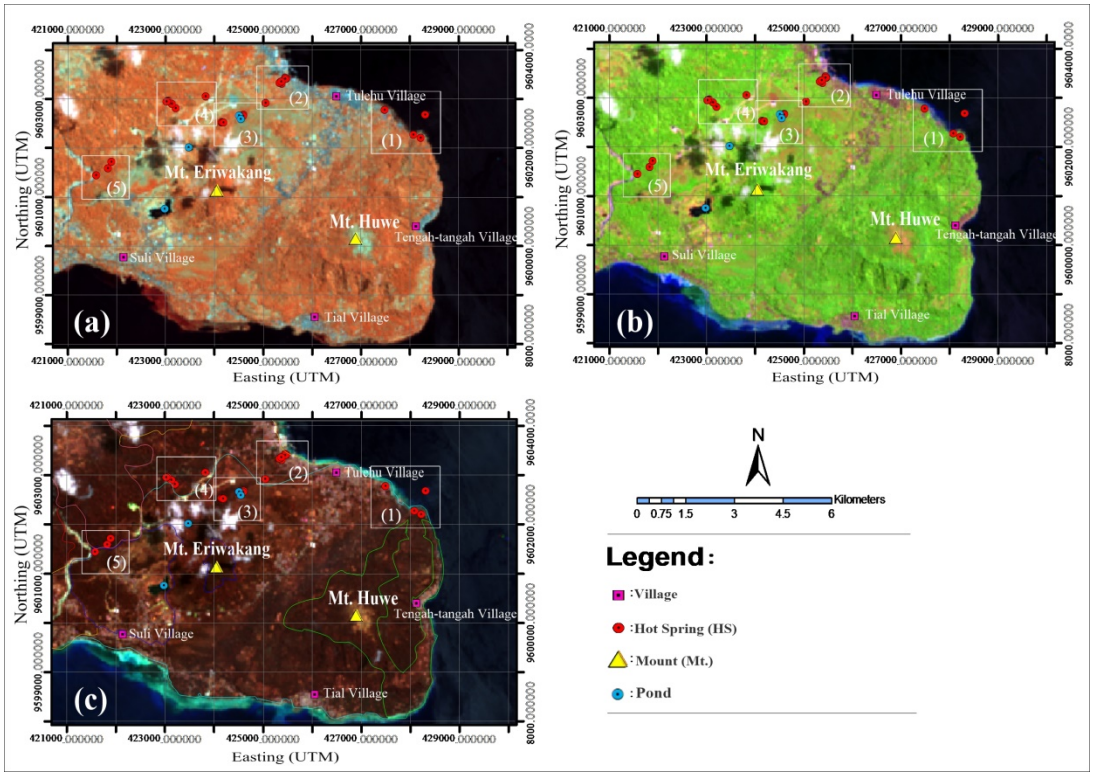

Fig. 7: (a) Composite map band-567, (b) Composite map band-653, and (c) Composite map band-742.

This composite band study will focus on five locations that have geothermal potential, namely: (1) Batu Kuda-Batu Lompa area, (2) Mamokeng area, (3) Sila-Telaga Biru area, (4) Hatuasa-Karkuri area, and (5) Hatuing area. The Batu Kuda area on the composite map band-567 can be seen if it looks brown in the south, which indicates vegetated land, while in the west and northwest, it is light green to light blue, which shows mixed land. The condition of the Batu Kuda area, when viewed on the composite map band-653, can be seen that in the southern part, it appears dark green, indicating forest areas. At the same time, in the west to the northwest, there is a mix of light brownish green and red colors, which show mixed land and residential areas. While on the composite map band-742, the southern part of this area appears brownish green to dark brown, which indicates vegetated land, while in the west and northwest, it appears dark brown and pink, which means mixed land and residential areas. The Mamokeng area on the southern, when viewed from the composite map band-567, seems brown and light green, indicating areas of mixed vegetation, while in the east to the north is dominated by a bright blue color indicating the location of a residential area. The hot springs in this area are seen on bare land, which is light green. The Mamokeng area, when viewed on a composite map band-653, can be seen in the southern part with a light green color, which shows a bush and mixed land. While, the eastern part is colored light brownish green and red, which indicates the location of a residential area, bare land, and grass. While the composite map of band-742, the southern part of the Mamokeng area appears to have a mix of dark brown and red to orange, which shows mixed land. Meanwhile, this area's eastern and northern parts appear pink, indicating a residential area's location. At a glance, the boundaries between alluvium deposit formations (Qa) and limestone units (Ql) can be seen at the area's southern end.

The Sila-Telaga Biru area, when examined through a composite map band-567, appears in the western part of this area in brown, which indicates a vegetated area; while in the eastern part, it tends to be light green which shows a location in the

form of mixed land and bare land. If examined using a composite map of band-653, the western part of the blue Sila-Telaga area is dark green to light green, indicating a vegetated area. In contrast, the eastern part is light brownish-green, showing a mixed land area. Meanwhile, when examined using a composite map-742, the western part of the Blue Sila-Telaga area is dominated by deep dark green, which indicates a vegetated area. In contrast, the eastern part is brown, which shows mixed land. The Hatuasa-Karkuri area, if viewed through the map of band-567, it appears that the area is dominated by reddish-brown color, and there are a few bright green dots in the east; thus, it can be said that this area is covered by vegetated land. The pixel with a bright green color is a bare land with few buildings. In addition, there are white colors on the east to the southeast, which indicate an open, sandy, and unpaved road. When viewed from the composite band-653, the Hatuasa-Karkuri area is covered by green color, and there is a slight light brownish green color on the southeast side which indicates mixed land. In addition, there are bright white colors pixels with an east to southeast direction, which shows a sandy open road. While, if viewed using the composite map-742, it appears that the Hatuasa-Karkuri area is dominated by dark green colors, which are vegetated land, with a few reddish-brown colors in the southeast, which are bare land. The same can be seen in the light yellow pixels with an east to southeast orientation indicating a sandy open path. On the composite map band-742, the boundaries of rock formations between alluvium deposit formations (Qa) and limestone units (Ql) are visible in the southern part of this area change in the color of the pixels from red to orange.

The Hatuing area, when viewed through a composite map band-567, appears that the area is dominated by reddish-brown color, which is vegetated land. There are a few bright green pixels in the southeast that indicate bare land. The hot springs in this area are located on vegetated land around the Yari River. If viewed on the composite map band-653, this vegetated area is dominated by green colors, while the area to the southeast is covered by orange-brown colors, which are bare land. While on the composite map band-742, the vegetated areas are in dark green colors, while the area's bare land is indicated by red to orange colors. Some hot springs in Hatuing area are located on the border of four rock formations, namely Dasitic lava unit (Tab), Simalopu pyroclastic unit (Tts), Eriwakang pyroclastic unit (Tte), and limestone unit (Ql). In addition, on the composite map band-742, the difference between the rock formations at the top of Mount Huwe is clearly visible, with the areas on the northwest, southwest, and east sides of the mountain. The difference is indicated by dark green and dark brown pixels, which indicate the boundary between limestone units (Ql) and Huwe pyroclastic units (Ttf).

c. Lineament Manual and Rosette Diagram

Surface geological structures such as faults in this study will be studied by constructing manual lineaments following the river valley lanes. The straight river valley and parallel valley segment are typical geomorphological expressions of lineament [16]. These lineament features can indicate the presence of geological structures in the form of faults. These faults are related to the emergence of geothermal manifestations in the study area, such as hot springs [19]. The manual lineament made on the DEM SRTM 2D map is used to create a rosette diagram that is useful for seeing the direction of the lineament distribution to the control of the dominant fault structure. In addition, the rosette diagram is used to investigate the direction of the dominant force that forms the topography of the study area.

Lineament analysis in this study focused on valleys with an azimuth of 45° and 135°. The manually drawing lineaments on the DEM SRTM 2D map with different azimuths will produce lineament segments with different orientations, just as the 45° azimuth will be different from the 135° azimuth. The lineament data of the DEM SRTM 2D map for the 45° and 135° azimuths inputted on the rosette diagram are shown in Figure 8 and Figure 9.

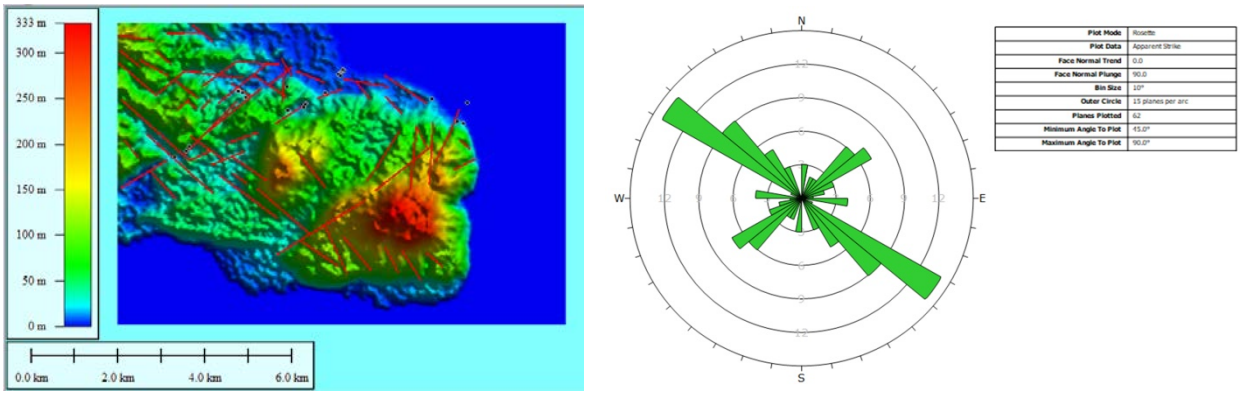

Fig. 8: (a) Valley lineament with azimuth 45°, (b) Rosette diagram of valley lineament with azimuth 45°.

Figure 8 (a) shows the valley lineament formed on the DEM SRTM 2D map with an azimuth of 45°. The valley lineaments that can be created based on the valley pattern in Figure 8 (a) are as many as 62 lanes with varying lengths and directions. While Figure 8 (b) is a rosette diagram as input result from the valley lineament data with an azimuth of 45°. Figure 8 (b) shows that the valley lineaments with an azimuth of 45° in the study area have a dominant northwest-southeast direction, with a slight concentration in the southwest-northeast area.

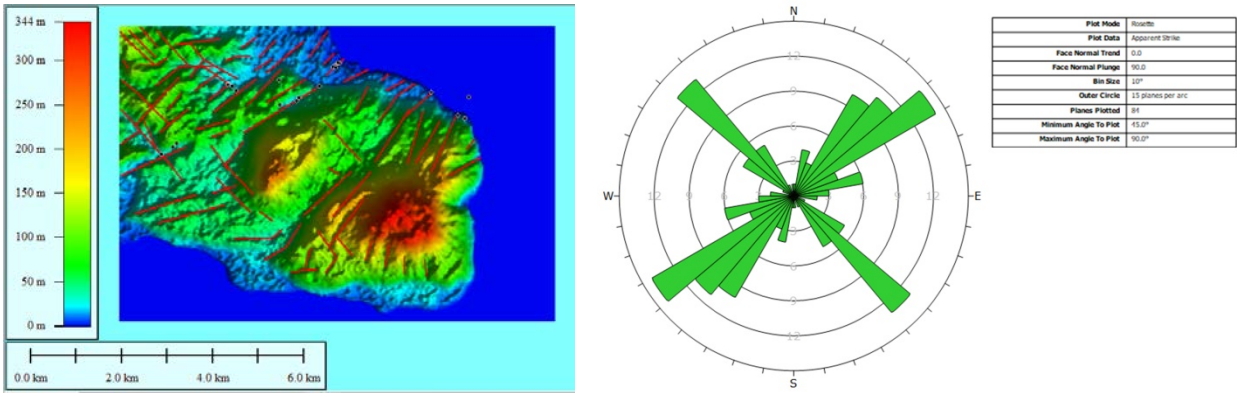

Fig. 9: (a) Valley lineament with azimut 135°, (b) Rosette diagram of lineament valley with azimuth 135°

Figure 9 (a) shows the valley lineament formed on the DEM SRTM 2D map with an azimuth of 135°. The valley lineaments that can be created based on the valley pattern in Figure 9 (a) are as many as 84 lanes with varying lengths and directions. While Figure 9 (b) is a rosette diagram as input result from the valley lineament data with an azimuth of 135°. Figure 9 (b) shows that the valley lineaments with an azimuth of 135° in the study area have a dominant direction with a southwest-northeast orientation; on the other hand, there is a slight concentration in the northwest-southeast area.

Based on the data in Figures 8 (b) and 9 (b), it can be interpreted that the force acting on the fault structures at the study area has a dominant trend in the direction of northwest-southeast and southwest-northeast. The dominant direction of the valley lineaments at the study area is directly controlled by the fault structures that cross the Tulehu area. The fault structures that cross Tulehu Village with a trend towards a northwest-southeast orientation are the Tulehu fault and the Huwe fault. Meanwhile, the fault structures that cross the Tulehu area with a trend towards southwest-northeast orientation are the Huwe fault, the Banda fault, and the Banda-Hatuasa fault. Thus, it can be said that the rosette diagram data for the valley lineament at 45° azimuth and 135° azimuth is positively correlated with the geological information of Tulehu.

5. Conclusions

Remote sensing methods can be used to cover all locations that have geothermal potential in Tulehu Village. The geothermal potential has been studied through land cover, land surface temperature (LST), and structural geomorphology. The study of land cover aspects is indicated by the NDVI value. The land cover condition in the study area from 2015 to 2017 had an average NDVI value of 0.380, 0.396, and 0.433, respectively. Meanwhile, the average LST value from 2015 to 2017 was 24.474, 20.743, and 25.167. The results showed that areas with a high LST anomaly trend were dominantly located on built-up land, residential complexes, and barren land. Locations with geothermal potential tend to have low LST anomaly trends because their manifestations are mostly in vegetated areas. Generally, the temporal changes of LST anomalies in the study area from 2015 to 2017 are influenced by changes in land cover. The geomorphological conditions of the structure in this study were assessed through surface morphometric maps, visual delineation on morphometric maps, composite band maps of Landsat-8 image, and manual lineament data extraction on rosette diagrams. The results of visual delineation on the morphometric map show a positive correlation between the valley lineament and the slope of the valley. The interpretation of the fault path through the valley lineament is greatly facilitated by monitoring the slope pattern of the valley on the morphometric 2D map. Surface geomorphological features such as geological structures, vegetation conditions (land cover), and rock minerals at the study site have been carried out using composite band maps of Landsat-8 image. The band-567 composite map can display features related to surface geological structures, such as river paths, valleys, and geological contact boundaries. The band-653 composite map can display surface features such as vegetation boundaries between dense vegetation, mixed vegetation, barren land, and residential areas. At the same time, the composite map of band-742 can display surface geological features such as differences in minerals or rocks and contact boundaries of

rock formations. In comparison, the manual lineament data extraction results on the rosette diagram show that the presence of geothermal manifestations in the study area is directly controlled/influenced by the presence of dominant fault structures with orientations of northwest-southeast and southwest-northeast.

Acknowledgments

The authors would like to thank the United States Geological Survey (USGS) for providing free satellite imagery data. The satellite images in intending are Landsat-8 satellite imagery and DEM SRTM 1 Arc Second imagery.

References

[1]. Jufri, A. Susilo., & Sunaryo., "Estimating Reservoir Rock Formation and Hood Stone in Manifestation Area of Tulehu Salahutu Healer – Ambon Island based on Magnetic Survey", Natural B, Vol. 3, No. 2, 2015, pp.158-165.

[2]. Japan International Cooperation Agency (JICA) preparatory survey for Tulehu geothermal power plant. Final Report. West Japan Engineering Consultants, Inc. (2011) I-1-VI-3.

[3]. Japan International Cooperation Agency (JICA)., Pre-Feasibility Study for Geothermal Power Development Projects in Scattered Islands of East Indonesia, *Study Report*. Engineering and Consulting Firm Associaton. Japan. (2007) 1-131

[4]. Putri, C.A.S. & Purwanto T.H., "Interpretation of Geological Structure and Lithology by Landsat-8 And SRTM Imagery in Rembang District and Its Surrounding. Jurnal Bumi Indonesia", 2015. Vol. 4, No. 3, pp. 1-10.

[5]. Herlambang, R.F. & Novranza, K.M.S., "Lineament Mapping Using Remote Sensing and Its Correlation to the Distribution of Surface Manifestations in the Kepahiang Geothermal Potential Area", Bengkulu. Prosiding Seminar Nasional Fisika (E-Journal) SNF2016, 2016. Vol. 3, No. 1, pp.57-64.

[6]. Roy, D.P., et al., "Landsat-8: Science and product vision for terrestrial global change research. Remote Sensing of Environment", 2014, Vol. 145, No. 1. pp. 154–172.

[7]. Siombone, S.H., Maryanto, S., & Wiyono., "Land Surface Temperature and Geomorphology of Tiris Geothermal Area, Lamongan Volcano Complex, Probolinggo, East Java, Indonesia. Environmental and Earth Sciences Research Journal", 2021, Vol. 8, No. 2, pp. 65-74. DOI**:** https://doi.org/10.18280/eesrj.080201

[8]. Azhari, A. P., Maryanto, S., & Rahmansyah, A., "Identification of geological structure and its effect on land surface temperature based on Landsat-8 data on the Blawan geothermal field", Jurnal Penginderaan Jauh dan Pengolahan Data Citra Digital, 2016, Vol. 13, No. 1, pp. 1–11.

[9]. Danoedoro P., Introduction to Digital Remote Sensing, Yogyakarta: Penerbit Andi, 2012. (In Indonesian)

[10]. Rumada, I.W., Kesumadewi, A.A.I., & Suyarto, R, "Interpretation of Landsat 8 Satellite Imagery for Identification of Mangrove Forest Damage in Ngurah Rai Forest Park, Bali", E-Jurnal Agroekoteknologi Tropika, 2015, Vol. 4, No. 3. pp. 234-243

[11]. Firdaus, H.S Ipranta, & Hani'ah., "Mapping of rock formations using Landsat 8 and Terrasar-X imagery (Case Study: Kota Batu, East Java)", ELIPSOIDA (Jurnal Geodesi dan Geomatika), 2018, Vol. 01, No. 01. pp. 12-19.

[12]. United States Geological Survey (USGS), Department of the Interior U.S. Geological Survey. Vol. 8, 2016.

[13]. Qin, Q., et al., "Geothermal area detection using Landsat ETM+ thermal infrared data and its mechanistic analysis-A case study in Tengchong, China. International Journal of Applied Earth Observation and Geoinformation", 2011, Vol. 13, No. 4, pp. 552-559.

[14]. Mia, M.B., Nishijima, J., & Fujimitsu, Y., "Exploration and monitoring geothermal activity using Landsat ETM+ images: A case study at Aso volcanic area in Japan". Journal of Volcanology and Geothermal Research, 2014, Vol. 275, pp. 14-21.

[15]. Mia, M.B., Fujimitsu, Y., & Nishijima, J., Thermal activity monitoring of an active volcano using Landsat-8/OLI-TIRS sensor images: A case study at the Aso volcanic area in southwest Japan. Geosciences, 2017, Vol. 7, No. 4, pp. 118.

[16]. Massinai. M.A., Tectonic Geomorphology, 2018, Yogyakarta: Pustaka Ilmu. (In Indonesian)

[17]. Van Zuidam R.A., Aerial Photo Interpretation in Terrain Analysis and Geomorphology Mapping, Netherland: Smits Publishers, 1985.

[18]. Fareka M.A, Sutarto N.R, & Pamungkas, T.D., "Slope Stability Analysis on Weathering of Volcanic Rocks in Cikalongwetan, West Bandung Regency, West Java". Jurnal Geografi Gea, 2020, Vol. 20, No. 1, pp. 26-28.

[19]. Iqbal, M & Juliarka, B.R., Analysis of Lineament Density as an indicator of the level of permeability in the Suoh-Sekincau Geothermal Field, Lampung. Journal of Science and Applicative Technology, 2019 3(2) pp. 61-67. DOI: 10.35472/jsat.v3i2.212

[20]. Lillesand, T.M., Kiefer, R.W., & Chipman, J.W., Remote Sensing and Image Interpretation (Fifth Edition), USA: John Wiley & Sons, 2004.

[21]. Li, Z.L., et al., "Satellite-derived land surface temperature: Current status and perspectives", Remote Sensing of Environment, 2013, Vol. 131, pp. 14–37. DOI: 10.1016/J.RSE.2012.12.008

[22]. Uddin. S., et al., "A remote sensing classification for landcover changes and micro-climate in Kuwait", 2010, ISSN: 1743-7601 (paper format), ISSN: 1743-761X (Online). DOI: 10.2495/SDP-V0-N0-1–11

Salman Hamja Siombone. He is a lecturer and researcher at STKIP Gotong-Royong Masohi. He took his undergraduate degree in physics education program, Pattimura University and completed it in 2015, then took a master's program at Brawijaya University Malang and completed his studies in 2019. His field of expertise is in physics, specializing in Geophysics, especially non-seismic geophysics and satellite imagery remote sensing. Currently, his research is more focused on geothermal physics and surface geomorphological structures. Two international scientific publications have been published, namely (1) Bouguer Anomaly of Geothermal Reservoir at Tiris Area, Probolinggo, East Java, Indonesia in the Journal of Geography, Environment and Earth Science International (JGEESI), and (2) Land Surface Temperature and Geomorphology of Tiris Geothermal Area, Lamongan Volcano Complex, Probolinggo, East Java, Indonesia in the Environmental and Earth Sciences Research Journal (EESRJ). He currently prefers to target his knowledge in geophysical research, especially in environmental and earth sciences.

Jufri. He is a lecturer in the Department of Mathematics and Natural Sciences at Darussalam University, Ambon. He was completed his postgraduate from Brawijaya University in 2015. His area of expertise is Geophysics. He has conducted several pieces of research in the geophysics field and physics education/teaching.

Wiyono. He is a lecturer in the Physics Department, Faculty of Mathematics and Sciences, Universitas Brawijaya. He was completed his Doctor program at Universitas Brawijaya.

U. M. Syaid Maba. He is a graduate of the Chemistry Study Program from the Faculty of Mathematics and Natural Sciences, Pattimura University, Ambon. He completed his studies in 2021 with a paper topic on the analysis of Lead (Pb) content in mangroves (Sonneratia alba) on the Lateri and Poka, Teluk Ambon Dalam.